EEET ECOLOGICAL ENGINEERING & ENVIRONMENTAL TECHNOLOGY

Ecological Engineering & Environmental Technology 2023, 24(8), 329–345
https://doi.org/10.12912/27197050/172225
ISSN 2719-7050, License CC-BY 4.0

Received: 2023.08.15
Accepted: 2023.09.17
Published: 2023.10.16

An Innovative Interaction between Organo-Kaolinite and Methyl Orange for Industrial Wastes Removal – A Kinetic Investigation and Modeling

Hussein A. M. Al-Zubaidi[1], Saif S. Alquzweeni[2], Safaa K. Hashim Al-Khalaf[3], Ahmed Samir Naje[4*]

[1] Department of Environmental Engineering, Faculty of Engineering, University of Babylon, Babylon, Iraq
[2] Department of Civil Engineering, Faculty of Engineering, University of Babylon, Iraq
[3] Collage of Engineering, AL-Qasim Green University, Babylon, Iraq; Faculty of Engineering, University of Kufa, Al-Najaf, Iraq
[4] Collage of Engineering, AL-Qasim Green University, Babylon, Iraq
* Corresponding author's e-mail: ahmednamesamir@yahoo.com

ABSTRACT

Since organic dyes are the main component of many industrial wastes, it is necessary to be removed efficiently and instantaneously. The aim of this research focuses on the synthesizing of organoclay by modifying kaolinite with cetyl trimethyl ammonium bromide and applying it for the removal of (methyl-orange) dye from water by the mechanisms of adsorption. The effects of several parameters, mainly agitation time, water pH, adsorbent doses, and dye concentrations, on the adsorption process were optimised using the central composite design (CCD) method, which was performed using MINITAB package (version 17). Results showed that the dye was completely (100%) removed at pH of 4.0, adsorbent dose of 0.4 g, dye concentration of 50 mg/L, and agitation speed of 160 rpm. In addition, it was found that Freundlich and Sips isotherms were the best models to track lab data. Moreover, the Pseudo second order method was found to be more convenient compared to other models for studying kinetics of the sorption mechanism. For column testing, an appropriate hydraulic conductivity and reactivity were obtained by combining modificatory kaolinite and glass waste with weight proportions of 50:50. Thus, empirical simulations such as those in the kinetic model of Clark have provided satisfactory consent for using the simulated methyl orange.

Keywords: modified kaolinite, cetyl trimethyl ammonium bromide, dye, insusterial wastes.

INTRODUCTION

Dyes are often employed in a variety of industrial processes to produce coloring, food, paint, fabrics, leathers, papers, and rubber. Dyes are often divided into natural and industrial dyes; the latter can be further divided into three categories: dyestuffs with anionic, cationic, and nonionic groups (Liu and Zhu, 2017). The aquatic eco-system may suffer as a result of the high dye concentrations in wastewater, which have been linked to severe illnesses including cancer. One of the most significant pollutants is the wastewater from various businesses, namely the industrial dyes industry, which contains organic chemicals. However, even in little amounts, the bulk of these dyestuffs are carcinogenic. Methyl orange is a water-soluble azo color that contains substances that cause cancer. Intestinal microbes break down this kind of dye into aromatic amines (Czaja et al., 2019), and its high stability, high solubility, and low biodegradability decrease the ability of conventional water treatment methods used to remove it from the solution. Many modern methods have been employed for dyestuff removal such as oxidation, membranes, and coagulants (Guo et al., 2023). Biological and chemical treatments have advanced significantly, but they still have several downsides, such as harmful byproducts of oxidation that are hard to

remove using conventional techniques (Guo et al., 2023). In the last few years, the biological treatment has given a high efficiency of dyestuff removal from wastewater without intermediate pollutants, but it still removes only the dissolved dyes (Guo et al., 2023). Adsorption is one of the most practical and affordable processes since the adsorbents are inexpensive and the results of the treatment are effective. In several investigations, dyes were typically employed to remove effluent from the chemical sector, including clay matter in various affordable or easily accessible adsorbents (Faisal et al., 2020). Nowadays, several industries use clay minerals broadly, such as in polymers nanocomposites adsorbents and adsorption of heavy metal ions (Sejie and Nadiye, 2016). The ratio of these sheets/layers in the structure is used to characterize clay minerals, which frequently have tetrahedral and octahedral layers. The clay is referred to as a 2:1 clay (3-sheets) if it consists of two tetrahedral layers and one octahedral layer. Similar to this, 1:1 clay (2-sheets) is defined as clay that has one octahedral layer and one tetrahedral layer (Sejie and Nadiye, 2016). The most common types of clay are montmorillonite, smectites kaolinite, and illite; however, montmorillonite and bentonite are largely used as an adsorbent in the exploration of the kaolinite clay mineral (Demeusy et al., 2023). The crystal structure of kaolinite was first set out by a model using an idealization of polyhedral. In this group, the clay minerals contain dioctahedral 1:1 layer structures with high $Al_2Si_2O_5(OH)_4$ in their composition. Due to the high concentration of octahedral sites, they are characterised by the predominance of Al^{+3} in spite of the presence of isomorphous substitutions of magnesium, iron, titanium, and vanadium ions for Al^{+3}. Some modifications, such as impregnation or the grafting of organic/inorganic molecules, can improve the characteristics of clay minerals. For instance, by adding quaternary ammonium cations to kaolin or montmorillonite, the effectiveness of the materials' ability to remove different organic contaminants is greatly increased (Ahmed et al., 2020, Faisal and Naji, 2019). In the this study, a new compound (CTAB-kaolinite), manufactured by modifying the kaolin by using cetyltrimethylammonium bromide (cationic surfactant), was applied to adsorb Methyl orange dye. Aditionally, isotherms of the adsorption processes were examined using Langmuir, Freundlich, and Sips models.

MATERIALS AND METHODS

Experimental work

Kaolinite used in this investigation was from an Iraqi source. It was natural and of particle sizes between 250 to 500 μm. The contaminants were the Methyl orange (anionic dye). In addition, one gram of colorant powder was added to one litter of denoized water to imitate polluted wastewater of 1000 mg/L. The modified kaolinite was formed in the natural sodium-kaolinite with a cationic surfactant to modify its form of hydrophilic to organophilic by substituting interchangeable sodium ions. Then, the adsorption behaviours, as an effectual adsorbent to remove the dye, were analytically examined. In the modification step, the organic cationic surfactant was ceyl trimethyl ammonium bromide (CTAB) provided by Sigma Aldrich Chemise (Germany). Also, the desired value of pH was mainained using suitable volumes of HCL or NaOH. Furhermore, the CCD technique was performed using the MINITAB 17 package to optimise the effects of the reaction parameters, namely treatment period (X_1) (63.75–181.25 minutes), pH of the solution (X_2) (4.5–9.5), adsorbent doses (X_3) (0.1575–0.4525 mg/g), methyl orange dye concentrations (X_4) (125–275 mg/L) and agitation speed (X_5) (62.5–187.5 rpm) on the dye removability by the CTAB-kaolinite.

Modified kaolinite preparation (organo-kaolinite)

The organic kaolinite was mixed with 50 mL of water that had been deionized for 120 minutes to swell and homogenize the kaolinite particles before being used to create the organo-kaolinite Jeeva and Zuhairi, 2018). After adding the necessary amount of surfactant (CTAB) in weight ratios of 0.05, 0.1, 0.2, 0.25, 0.3, 0.35, 0.4, 0.45, and 0.5 g CTAB for each gram of kaolinite, the mixture was well mixed for two hours. The final sample (combination) was known as modified kaolinite (organoclay), and it was dried at 105 oC after undergoing a series of washing procedures with deionized water to remove the remaining salt. At sieves of 250–500 m, the modified kaolinite samples were crushed and tamed. In subsequent testing, the specimen with the specified dose of CTAB had the greatest dye concentration.

Batch mode sorption experiments

By using batch experiments under different conditions, the modified kaolinite has been used to study methyl orange dye adsorption. The experimental work started by applying to 100 mL of the synthetic solutions of methyl orange colour the desired amount of modified kaolinite. Then a thermostatic shaker shaked the mixture (Edmund Buhler SM25, German). Diverse touch periods, starting pH (2–12), stirring rates, sorbents doses (0.01–0.6 g/100 mL) were taken for batch tests in various contact times (0 to 240 minutes). A suitable volume of the solution was periodically taken and then qe ($mg.g^{-1}$) was calculated as follows (Naji et al., 2020, Abd Ali et al., 2020):

$$q_e = \frac{(C_. - C_f)V}{m} \tag{1}$$

The removal efficiency (*R%*) of dye using CTAB-kaolinite has been determined using the following equation (Alshammari et al., 2020):

$$R\% = \frac{(C_. - C_f)}{C_f} \times 100 \tag{2}$$

Kinetic study

Pseudo-first-order model

It describes the adsorption concentrations of dissolved chemicals by the solution. formula (Faisal et al., 2020, Ahmed et al., 2020):

$$\frac{dq}{dt} = k_1(q_e - q_t) \tag{3}$$

Integrating Eq. 3 at two conditions, which are q_t=0 when t=0 and q_t=q_e when t=t, yields the following form of the model:

$$q_t = q_e * (1 - e^{-k_1 t}) \tag{4}$$

Pseudo-second-order model

This model is based on a number of assumptions, including 1) a monolayer could be formed on the surfaces of the adsorbent by attaching pollutants, 2) the sorption energy is constant for each adsorbent, and 3) there are no interactions between the adsorbed pollutants. it could be expressed by the following formula (Faisal et al., 2020):

$$\frac{dq}{dt} = k_2(q_e - q_t)^2 \tag{5}$$

Integrating Eq. 5 at two conditions, which are q_t=0 when t=0 and q_t=q_e when t=t, yields the following form of the model:

$$q_t = \frac{t}{\left(\frac{1}{k_2 q_e^2} + \frac{t}{q_e}\right)} \tag{6}$$

Intra-particle diffusion

This model was proposed for the first time by Weber and Morris (1962) and received a big deal of attention due to its ability to explain the adsorption process. The general form of this model is:

$$q_t = k_i t^{\frac{1}{2}} + C \tag{7}$$

where: ki and i – represent the model constant ($mg/g \cdot hr^{1/2}$) and the slope of the relationship between qt and $t^{1/2}$, respectively.

The numerical value of i equals to C, which indicates how much the boundary layer is thick. Thus, it could be concluded that when the value of the intercept is large, the effect of the boundary layer could be easily recognised. The intra-particle diffusion occurs when the relationship between qt and $t^{1/2}$ is linear. Only intra-particle diffusion is represented the rate-limiting process when the linear plot goes through the origin. Otherwise, the intra-particle diffusion should consider another mechanism.

Sorption isotherms

The adsorption process is typically represented using isotherms, which are also used to describe the equilibrium relationships between the concentrations of adsorbates in the fluid phase and the adsorbent at an appropriate temperature. The isotherm parameters could be estimated by plotting the weight of adsorbate qs in the particles of adsorbent against the concentration (C_e). For comparison purposes, mass normalization (mass of adsorbent) was applied to describe the quantity. The sorption capacity is improved with the increase of concentration but is not necessary to follow direct proportions. The convex upward type of isotherm is favourable due to the relatively high solids loading, which could be attained at low concentrations. Concave upward isotherm types are unfavourable as it has a relatively low solid loading and quite long mass transferring zones. The isothermas flow through the origin as they are linear and the adsorbed concentration is proportionate to the concentrations in the solution. These curves demonstrate that desorption is a special property which

relies on the structure of the adsorbent device. The irreversible isothermal is the favored form of adsorption, because it depends on the volume of adsorbed solvent as it falls to very low levels. The following isotherms were used.

Model of Freundlich

Originally, this model was empirical but after that, it was interpreted because of the need to study the adsorption processes on heterogeneous surfaces at different affinities. This model based on a number of assumptions; the stronger binding site is firstly occupied, and the strength of the binding declined as the level of site occupation increases. The general form of this model is:

$$q_e = K_F C_e^{1/n} \; n > 1 \tag{8}$$

where: n – an empirical coefficient, K_F – the coefficient of the model (Miz et al., 2014, Saad et al., 2019).

Model of Langmuir

This model assume the saturated monolayer of solutes molecules on the adsorbent surface is associated with the maximum degree of adsorption, and presupposes that both the energy of adsorption and the adsorbate. This model is suitable for single-layer adsorption, and it could be represented in the following equation (Alquzweeni et al., 2021).

$$q_e = \frac{q_m b C_e}{1 + b C_e} \tag{9}$$

Sips isotherm

This model could be defined as a hybrid model that utilises both Langmuir and Freundlich models. It has a good ability to depict the heterogeneous surface in comparison with other models. It follows the Freundlich model at low concentrations of adsorbates, but it behaves similar to the Langmuir model at high concentrations of adsorbates. The general formula of this model is (Ahmed and Dhedan, 2012):

$$q_e = \frac{q_m (b C_e)^{\frac{1}{M}}}{1 + (b C_e)^{\frac{1}{M}}} \tag{10}$$

Continuous mode sorption experiments

The column Perspex was employed to create the continuous adsorber that was used in this experiment. The column is 50 cm long and 2.5 cm in diameter, with a wall thickness of 5 mm (Figure 1). Column tests are intended to depict how the permeable reactive barrier actually works by allowing for standardized water flow and 1D pollutant migration. The columns have been packaged with organocaolinite only without any aquifer since the purpose of the continuous experiments is to determine the usefulness of this substance as a permeable reactive obstacle to the removal of the concentration of the contaminant. At room temperature, the packaged bed was supplied with purified water from the base of the columns. The polluteated water was inserted into the column with a certain flow rate value at constant hydraulic gradient after the bed had been saturated with distillated water. Port1 is fitted with 50 cm from the base of the column with each column (Figure 1). Metal concentrations were monitoring in effluents for 160 hours and samples could be regularly withdrawn and deposited in the glass vails.

In light of the aforementioned, organo-Kaolinite has a lower hydraulic conductivity than more conventional reactive media. Therefore, by mixing the organokaolinite with coarse materials like sand, coarse sand, or tyre chips, the significance of organokaolinite hydraulic conductivity should be increased to larger than conventional norms (Al-Zubaidi, 2012, Naji et al., 2020). Based on the idea of protecting and reusing environmental trash, glass debris was gathered, cleaned, crashed, and tampered with (0.35 mm), and it was then blended with modified bentonite to increase hydraulic conductivity and prevent the sofa from being obstructed. In the column tests however the modified bentonite was combined with a glass waste by two checked reactive systems. The method consisted of 1/1 blending organo-chaolinite and glass waste (0.00865 cm/sec).

A Transport Equation of contaminant shall be added to complete the hydraulic and geochemical output vision, to determine and choose the best method of action in permeable reactive barrier Three mechanisms regulate the flow of reactive pollutants in pore media: traveling water advection, hydrodynamic dispersion and soil adsorption or mass exchange. The simultaneous solution of the advective-dissipation transport equation and the equation defining the relationship of the solution and the soil matrix which be used to model the reactive contaminant transportation through porous media. The following is a representation of the one-dimensional advection-dispersion equation:

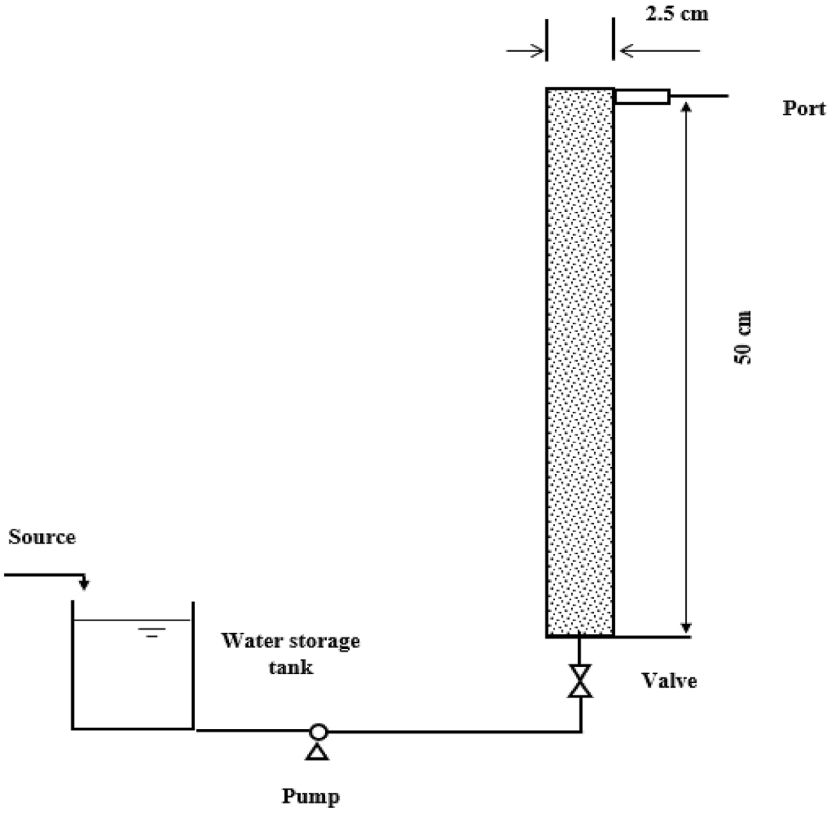

Figure 1. Laboratory-scale column schematic diagram

$$n\frac{\partial C}{\partial t} = nD_z\frac{\partial^2 C}{\partial z^2} - nV_z\frac{\partial C}{\partial z} - \rho_b\frac{\partial (q)}{\partial t} \quad (11)$$

where:

$$q = function\ (C) \quad (12)$$

Eq. 11 can be written with respect to the feature sorption (or adsorption isotherm):

$$\frac{\partial C}{\partial t} = \left(\frac{D_z}{R}\right)\frac{\partial^2 C}{\partial z^2} - \left(\frac{V_z}{R}\right)\frac{\partial C}{\partial z} \quad (13)$$

where: R – the retardation factor and defined as:

$$R = 1 + \frac{\rho_b}{n}\frac{\partial q}{\partial C} \quad (14)$$

The flow value of the flow domain at all points z and t is represented by the Equation 13 solution as in the continuous laboratory column examination. This solution is called the groundbreaking contaminant curve. The confirmation is carried out by experimental results collected on the scale of laboratory columns and a phenomenology of such curves is predicted. The breakthrough curve is S-shaped with a steady and continuous influential contaminant. The following is a description of the analytical and theoretical models used in the analysis (Naji et al., 2020).

Model of Bohart-Adams (1920)

One of the first essential mathematical equations was established by Bohart and Adams as the connection between normalized C/C0 concentration and time in a one-dimensional sorting system.This model takes the following form (Faisal et al., 2020):

$$\frac{C}{C_0} = \frac{1}{1 + \exp\left(KN_0\frac{Z}{U} - KC_0t\right)} \quad (15)$$

Yan Model (2001)

A highly reliable predictive model structure was used to present experimental results with some simplifications (Yan et al., 2001):

$$\frac{C}{C_0} = 1 - \frac{1}{1 + \left(\left(\frac{0.001 \times Q \times C}{q_0.M}\right) \times t)\right)^a} \quad (16)$$

where: q_0 and a can be calculated for experimental breakthrough curve data by non-linear adjustment of Equation 17. This model was renowned for the dose response model, see (Chatterjee and Schiewer, 2014).

Model of Clark (1987)

According to Clark, piston flow is of the same kind and the sorption motion of the pollutant is dependent on the Freundlich isotherm (Chatterjee and Schiewer, 2014):

$$\left(\frac{C}{C_0}\right)^{n-1} = \frac{1}{1 + A \cdot e^{-rt}} \quad (17)$$

RESULTS AND DISCUSSION

Characterisations of adsorbent

The FTIR measurement was used to differentiate between the surface functional groups on kaolinite and CTAB-kaolinite between 4000 and 400 cm^{-1}, as shown in Figure 2. The observed broad absorption band on the kaolinite at 3781 is because of the O-H stretching in the silanol. The Si-O-Si family of the tetrahedral layer is shown by the strong bands at 1027 and 792 cm^{-1} (Guo et al., 2023). CTAB-kaolinite samples showed additional absorption connections at 2937, 2842, and 1472 cm^{-1}. These bands presence is proof that CTAB has been incorporated into the clay's crystalline structures. As CTAB loading was increased, it was observed that the peaks of the CTAB-kaolinite at 2935 and 2848 cm^{-1} were intensified and their peak area was maximized. The CTAB molecules were intercalated between the layers of the kaolinite material, as shown by the presence of CH_3 and CH_2 groups. The surface alteration of kaolinite employing CTAB has also been performed, according to FTIR data (Anirudhan and Ramachandran, 2015, Faisal et al., 2020). SEM analysis has been used to examine the surface morphology and microstructure of unaltered natural kaolinite (Figure 2). The results of the SEM revealed that the surface morphology of natural kaolinite underwent significant changes after being modified; whereas the surface of natural kaolinite is porous and irregular, the surface of modified kaolinite is smooth with few holes (Guo et al., 2023). The SEM images of the CTAB-kaolinite also show that larger block structures have been formed from small pieces of the crimp and natural kaolinite, which possibly occurred because of the reductions in certain amorphous phases (Guo et al., 2023, Anirudhan and Ramachandran, 2015). At $P/P_o > 0.4$, isotherms of adsorption/desorption for the two materials rose gradually and they didn't stay overlaid, showing a dramatic lag phenomenon of retraction. In the system of pore filling Hysteresis loop was visible. The explanation of this phenomenon was the absence of clear adsorption limits for a flake-shape particle material or a crack hole material

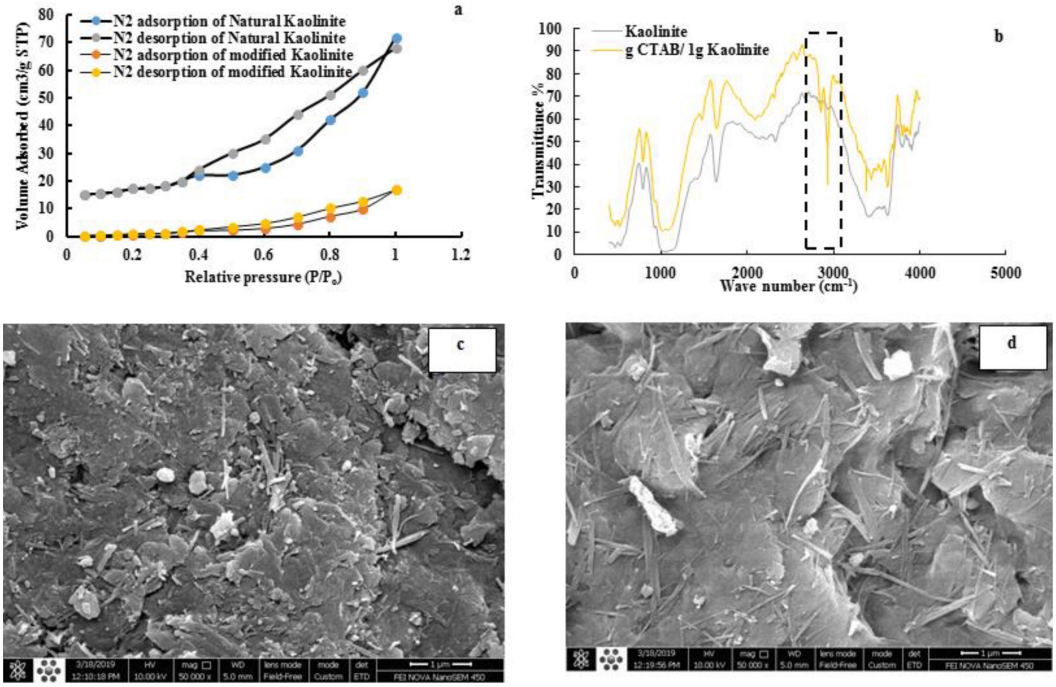

Figure 2. Results of: (a) N_2 adsorption-desorption isotherms, (b) FTIR, (c) SEM of Na- kaolinite, and (d) SEM of CTAB- kaolinite

in the relatively high-pressure areas. Both of the Na-kaolinite and organoclay isotherms have good adsorption capacities that help to reach gradually to the linear branch at high relative pressures, and the round-knee at low pressures. The enhanced adsorption of nitrogen in the wider micropore and mesopore is the reason for the higher surface area of Na-kaolinite. It was noticed from the adsorption data at P/P0 of 0.95 that the total pore volume was 0.32 mL/g in Na-kaolinite and 0.21 mL/g in organoclay. Due to the neutralisation reactions, the CTAB and the negative charges of the Na-kaolinite surface have occurred. Additionally, it was noticed that the products of reactions accumulated on the surfaces of the kaolinite that significantly decreased its surface area. In summary, the outcomes of the BET analysis unveiled that the surface area, pores volumes, and pores sizes of the CTAB-kaolinite (32.77 m^2/g) was lower than that of the modified kaolinite (73.61 m^2/g), which could be a result of the movement of the CTAB molecules into the interlayers of kaolinite and engaged its surface causing the blocking of the channels in the middle of the layers, and consequently decreases the area of surface, pores volumes, in addition pores sizes.

Modification of kaolinite

As shown in Figure 3, various adsorbent samples were created and tested by mixing various concentrations of CTAB with a predetermined amount of natural kaolinite (g CTAB/1g of natural kaolinite) under predetermined conditions:

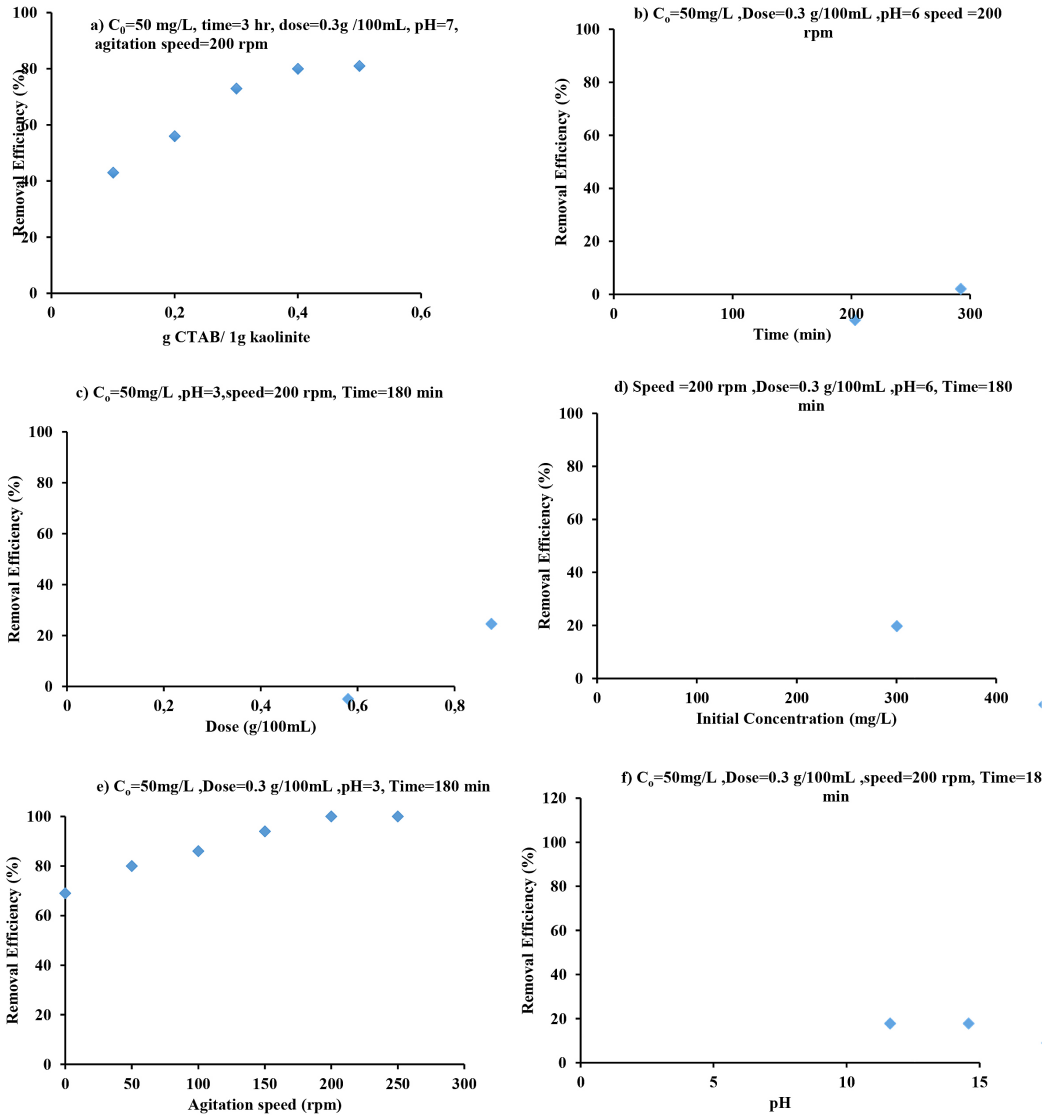

Figure 3. (a) Effects of the ratio of CTAB/ kaolinite (b) Equilibrium time (c) dosage (d) initial concentration, (e) speed (c) , and (f) Initial pH

Concentration of 50 mg/L, treatment time of 3hr, pH of 7, agitation speed of 200 rpm, and dose of 0.3g. When the amount of CTAB was reduced, it was found that the dye removability increased. The presence of the cations from the modified kaolinite and the methyl orange dye, which produce an electrostatic repulsion force, may be responsible for this behavior. In order to get the greatest dye removal percentage (80%), a 0.4 g CTAB/g percentage was selected as the ideal ratio for this adjustment. Under the same conditions as above, natural kaolinite was also tested for its ability to remove the color methyl orange, and a 30% clearance rate was noted.

It was discovered that the modified kaolinite can adsorb the methyl orange color 2.6 times better than the native kaolinite. This rise resulted from the kaolinite layer's spacing expanding following alteration that changed the hydrophilic surface of the kaolinite to a hydrophobic one, increasing the adsorptive characteristics. To prompt the kaolinite intercalated reaction, the applied doses of quaternary ammonium salts were increased as the ideal status cannot be achieved in practice. The variation of the methyl orange dye adsorption with the amounts of CTAB is displayed in Figure 3, which confirms that the existence of the cationic surfactant (CTAB) exerts noticeable effects on the adsorption of dye on kaolinite.

Batch outcomes

To explore the kinetics and behaviour of dye adsorption, several experiments have been carried out at different parameters namely, treatment period, pH of the solution, adsorbent doses, methyl orange dye concentrations, and agitation speed. Figure 3 shows the time effects on the removal of methyl orange dye using the modified kaolinite (0.3 g/100 mL). Clearly, the removability of the methyl orange dye has obviously increased with contact time. At the treatment begining , the sorption rate was fast and then it slowed increasingly until it reached the equilibrium status. This slowness of sorption is believed to be due to the decrease in the active sorption surface sites of the modified kaolinite with the time that results in limited adsorption. The experimental data showed that 85% of methyl orange dye was removed during the first 180 min. After the equilibrium time, there were no significant improvements in dye residual concentration (180 minutes). The effects of the initial concentrations of the methyl orange dye on the sorption onto modified kaolinite are displayed in Figure 3 that the removed percentage of the methyl orange dye has decreased from 85% at a dye concentration of 50 mg/l to 53% at a dye concentration of 350 mg/L. This decrease in dye removal indicates that soption capacity of the modified kaolinite decreased with higher dye concentration. The initial pH is one of the key factors in the sorption since it affects the adsorbent's capacity. As a result, the sorption of the methyl orange dye on modified kaolinite was evaluated at 50 mg/L and 0.3g doses at various pHs (ranging from 2 to 12). Using the appropriate amounts of HCL or NaOH, the correct pH was achieved. Figure 3 showed that when pH increased, the sorption process for the methyl orange dye reduced. This is explained by the fact that at high pH levels there were less positive charges on the surface of modified kaolinite, while there were more negative charges. These results concur with those of other researchers who have demonstrated that an increase in pH causes a reduction in the sorption of anion dyes. Figure 3 shows that at pH of 3, the highest amount of methyl orange dye could be removed, which was 100%. The dependence of methyl orange dye sorption on sorbent dose was investigated by adding several quantities of the modified kaolinite (0.01, 0.05, 0.1, 0.2, 0.3, 0.4, 0.5, 0.6 g) to 100mL of contaminated solution at room temperature and at speed = 200 rpm, C. = 50mg/L, pH = 3, and time = 180 minutes. Figure 3 presents the methyl orange dye removal percent as a function of the modified kaolinite doses. The removal percent improved with increasing the sorbent dosage, for example, the removal of methyl orange dye increased from 68 at a sorbent dosage of 0.01 mg/l to 100% at 0.3 mg/l sorbent dosage, and then the removal percent remain approximately constant afterward. The increase in the amount of adsorption site, as the dosage of sorbents increases, leading to more sorption sites, are responsible for this behavior.Moreover, after a certain dosage of sorbent was added to the solution; the amount of methyl orange dye engaged to the sorbent will not increase even if the treatment time increased (Kıranşan et al., 2014, Fosso-Kankeu et al., 2016). The effects on the methyl orange dye removal were investigated at various speeds (0-250) rpm, keeping other parameters constant. Figure 3 demonstrates how the amount of methyl orange dye removed rose from 69% to 100% when the agitation speed was increased from 0 to 200 rpm. High agitation speeds may enhance contaminant

diffusions towards the surface of the adsorbents, which leads to good contact between the sorbates in solution and the binding sites and an efficient sorbate transfer to the available adsorption sites.

Kinetic behavior

Based on Figure 4 and Table 1, and to find the difference between the calculated results (q_e) and the experimental results (q) of organo-Kaolinite on the removal of Methyl orange, both of the calculated results (q_e) and the experimental results (q) of the pseudo-first-order kinetic model, pseudo-second-order kinetic model, and intra-particle diffusion model were compared according to values of correlation coefficient (R^2) (Al-Zubaidi and Wells, 2020). It is clear that the best description of the adsorption process could be provided by the pseudo-second-order kinetic. Plots of versus $t^{1/2}$ for the intra-particle diffusions model are depicted in Figure 4. When the values of R^2 are relatively high, the plots become linear (Table 2). However, these straight plots did not go through the origin and refer to the involvement of intra-particle diffusion with the adsorption process but it is not the rate-controlling step. In addition, the plots of intra-particle diffusion show multi-linearity (Figure 4), and two or more mechanisms instantaneously occur and control the adsorption of Methyl orange dye. As shown in Figure 4, the increase in rate parameters in all portions occurred as the initial concentration increased, and this may be explained as applying Fick's Law in the intraparticle diffusion model. As a higher concentration gradient was applied, the diffusion became faster and adsorption was quicker, which explains the more required time for the adsorbent to reach the equilibrium status with a higher initial concentration of pollutants (Al Juboury et al., 2020).

Sorption isotherms

It is distinct that the Freundlich and Sips formulas provided good correlations for methyl orange dye adsorption compared to other models, as shown in Figure 5. Thus, these models have been employed to explore the adsorption of methyl orange dye on the modified kaolinite.

Response surface design

The required limits of the selected operating parameters to perform the response surface design

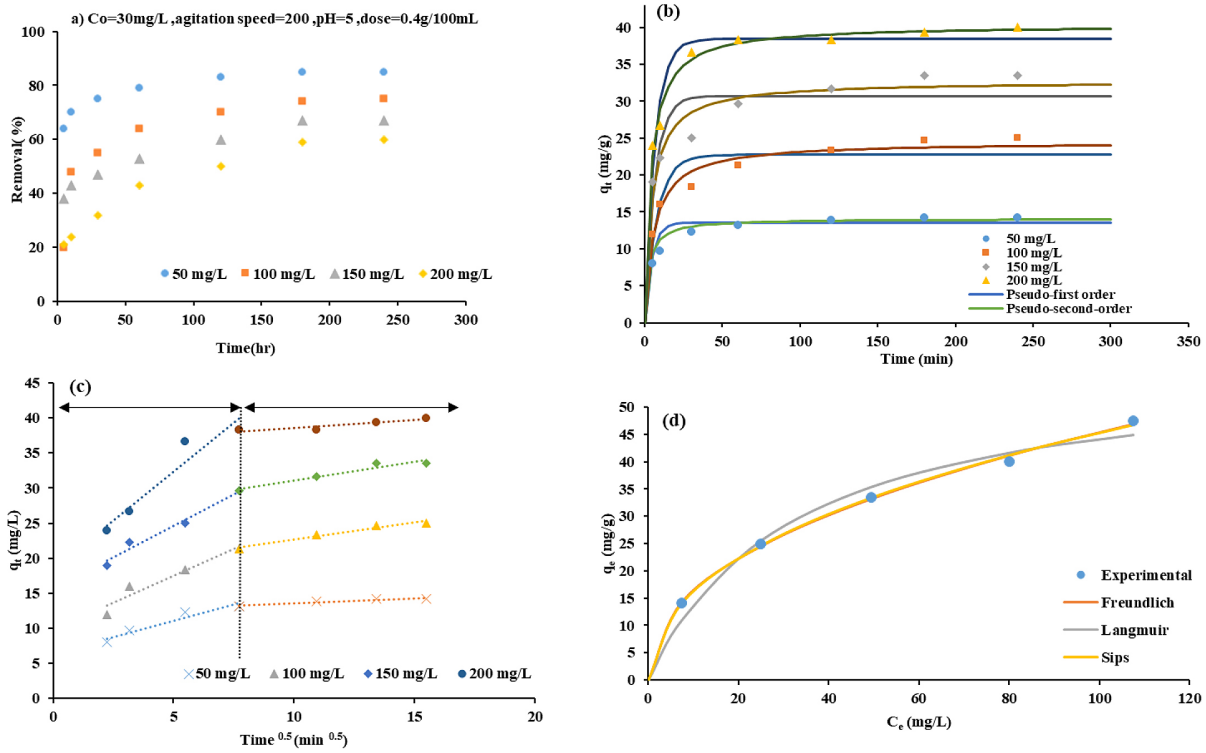

Figur 4. (a) Effect of contact time with different concentration represent as adsorption capacity (mg/g) (b) Pseudo-first-order, Pseudo-second-order, (c) interparticle diffusion and (d) sorption isotherms

Table 1. Kinetic and isotherm model of methyl orange on organo-kaolinite

	Model		Constant	Kaolinite
kinetic model	50 mg/L	Pseudo-first-order	k_1	13.539
			q_e	0.221
			R^2	0.834
			SSE	9.226
		Pseudo-second-order	q_e	14.075
			k_2	0.029
			R^2	0.979
			SSE	5.341
	100 mg/L	Pseudo-first-order	k_1	22.736
			q_e	0.127
			R^2	0.808
			SSE	28.194
		Pseudo-second-order	q_e	24.491
			k_2	0.007
			R^2	0.941
			SSE	8.532
	150 mg/L	Pseudo-first-order	k_1	30.696
			q_e	0.156
			R^2	0.726
			SSE	56.3
		Pseudo-second-order	q_e	32.718
			k_2	0.007
			R^2	0.9
			SSE	20.144
	200 mg/L	Pseudo-first-order	k_1	38.433
			q_e	0.153
			R^2	0.899
			SSE	28.95
		Pseudo-second-order	q_e	40.328
			k_2	0.006
			R^2	0.965
			SSE	9.12
Sorption isotherms	Langmuir		q_m	58.2296
			b	0.03135
			R^2	0.97149
			SEE	22.8827
	Freundlich		n	2.25678
			kf	5.89834
			R^2	0.99708
			SEE	1.96724
	Sips		q_m	367.579
			b	0.000173
			M	2.067914
			R^2	0.999826
			SEE	2.15739

Table 2. Parameters of Intra-particle diffusion

C. (mg/L)	Parameter	Part I	Part II
50 mg/L	k (mg/g min $^{0.5}$)	2.7705	0.2248
	C	18.519	36.324
	R^2	0.9187	0.8426
100 mg/L	k (mg/g min $^{0.5}$)	1.798	0.5298
	C	15.63	25.778
	R^2	0.9721	0.9336
150 mg/L	k (mg/g min $^{0.5}$)	1.5335	0.4892
	C	9.7776	17.761
	R^2	0.9254	0.9608
200 mg/L	k (mg/g min $^{0.5}$)	0.9307	0.1341
	C	6.4589	12.237
	R^2	0.9288	0.8995

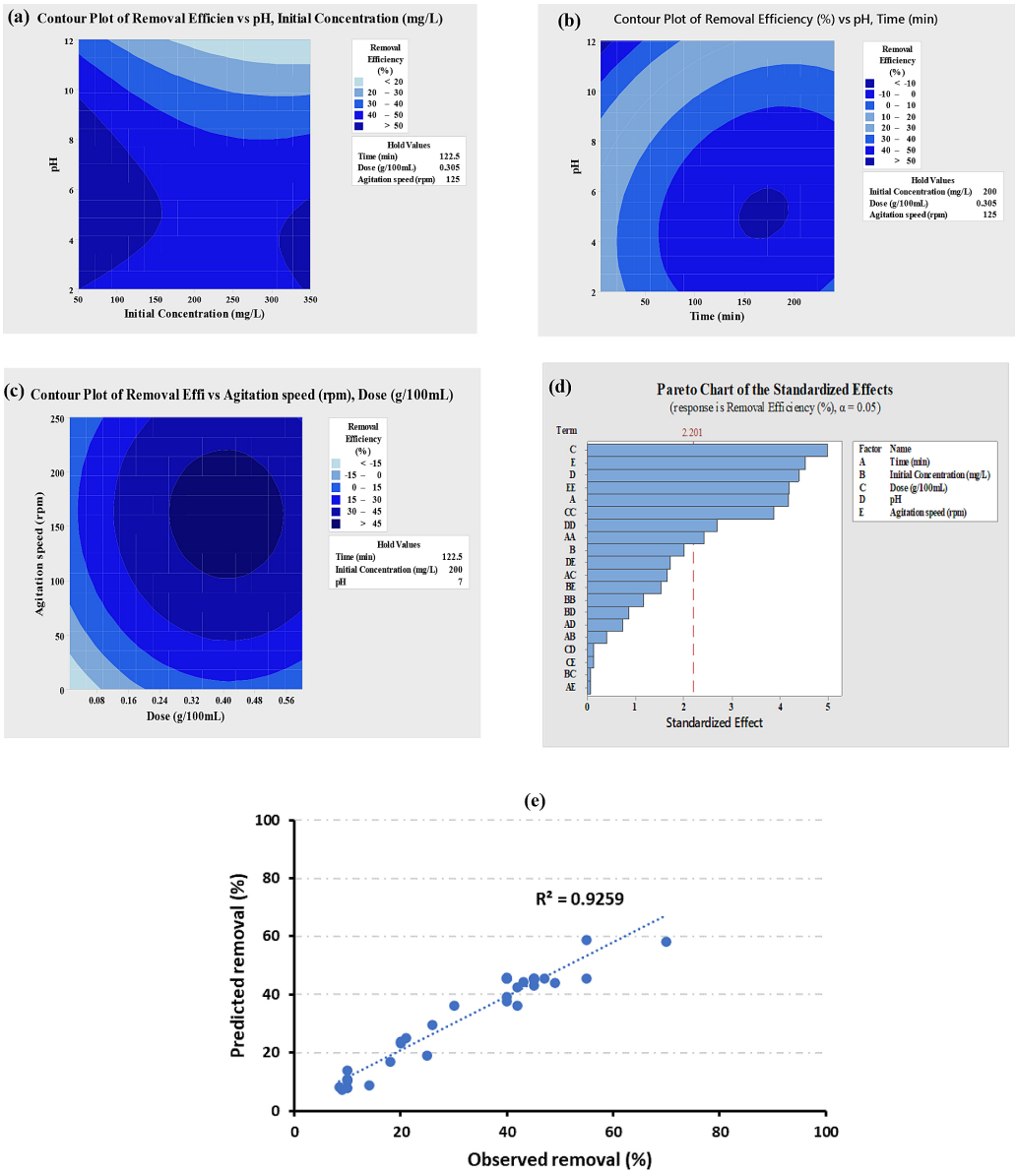

Figure 5. Contour plots for the outcomes of the developed CCD model (a, b and c), Pareto chart for standardized effects (d), and Observed vs predicted removals of Methyl orange using the modified kaolinite (e)

are shown in Table 3. To optimise the impacts of these parameters on the adsorption process on the modified kaolinite, the design of experiments was carried out, see Table 4 for the observed outcomes. These results were applied to the CCD to develop a predicting model, as shown in Eq. 18 based on (Al-Zubaidi et al., 2021).

$$\begin{gathered}\text{Removal (\%)} = -38.3 + 0.144X_1 - 0.196X_4 \\ + 155.1X_3 + 8.70X_2 + 0.520X_5 - 0.000980X_1^2 \\ + 0.000287X_4^2 - 247.5\,X_3^2 - 0.601\,X_2^2 - \\ 0.001494\,X_5^2 + 0.000170\,X_1X_4 + 0.361\,X_1X_3 + \\ 0.0094\,X_1X_2 - 0.000034\,X_1X_5 + 0.011\,X_4X_3 \\ -0.0087\,X_4X_2 + 0.000613\,X_4X_5 + 0.68\,X3X_2 - \\ 0.027\,X3X_5 - 0.0208\,X_2\,X_5\end{gathered} \quad (18)$$

This model was used to predict the adsorption of dye on the modified kaolinite, as illustrated in Table 3, which approves that the observed and the forecasted results follow a similar pattern. Additionally, Figure 5 indicates that the R^2 for the relationship between the observed and the predicted results is 0.9259, which also confirms a good correspondence between these results. Results of Table 3 and Figure 5 could be used as evidence for the applicability of the CCD technique to optimise the impacts of the operating parameters on the adsorption of the dye on the modified kaolinite. Figure 5 displays the contours plots for the outcomes of the developed model (Eq. 18).

Exploration of variance

As it stated in the previous section of this investigation that a CCD design for time (5-240 minutes), pH (2-12), speed of agitation from (0-250 rpm), dose (0.01-0.6 g/100mL), and initial dye concentration (50-350 mg/L) was conducted, which indicated that 32 runs are required to have a reliable design. The analysis of variance (ANOVA) results for this CCD design is shown in Table 5. According to the ANOVA results, the studied parameters exerted dramatic influences on the adsorption capacity because the statistical significance of the pH and the initial dye concentration was 0.015 and 0.269 (less than 5%), respectively (Al-Jassani et al., 2022). The pH and initial teinting concentration for interaction in the second order are also greatly affected, as the value of p was 0.406 ($p < 5\%$). This indicates that the best outcomes of this experiment needed to be checked, since the relationship was the main influence of the regulated variables. The pH and initial concentration associations have varying consequences. For lower values of the initial dye concentration, the relationship continues to show a significant positive influence, whereas it decreases near to zero for a value of initial dye concentration of 50 mg/L.

When the initial dye concentration rises above 300 mg/L, the interaction shows negative effect to the adsorption power. The adsorption potential demonstrated a non-linear behavior at a pH of 4 and initial dye concentration of around 50 mg/L. The results of the ANOVA used to verify the significance and suitability of the regression model derived by CCD are shown in Table 5. Fisher's and null hypothesis tests were used to determine the significance of the regression model and each coefficient term in light of the obtained F and P values (Reddy and Lee, 2013). Generally speaking, a higher F value and lower P value indicate that the regression model and each coefficient are more significant (Ahmad, 2013). Additionally, Table 5 shows that the model has significant significance as indicated by the greatest F (6.87) and lowest P (0.001) values, respectively. Additionally, due to the high values of F (17.25, 8.33, and 0.96) and the low values of P (0.00, 0.002, and 0.524), the principle coefficients, such as linear, square, and quadratic coefficients, have large significances. The p-value is more than 0.05, indicating that the lack of fitness is not significant. The correlation coefficient R2 has been used to evaluate the suitability of the proposed model. The R2 score, which indicates a comparable pattern between experimental and anticipated values of the response, was 92.59, according to the ANOVA data. The importance of the interplay between the initial dye concentration and pH can also change the major influence of the

Table 3. Studied limits of the selected operating parameters

Factor	Name	Low	High
X_1	Time (min)	63.75	181.25
X_2	pH	125	275
X_3	Dose (g/100mL)	0.1575	0.4525
X_4	Initial concentration (mg/L)	4.5	9.5
X_5	Agitation speed (rpm)	62.5	187.5

Table 4. Design of experiments with observed and predicted removals of methyl orange dye using the modified kaolinite

Time (min)	Initial concentration (mg/l)	Dose (g/100ml)	pH	Agitation speed (rpm)	Experiential elimination (%)	Predicted elimination (%)
122.5	200	0.6	7	125	40	39.31
122.5	200	0.305	7	250	42	36.11
181.25	125	0.4525	4.5	187.5	55	58.65
63.75	275	0.1575	9.5	187.5	10	10.81
63.75	125	0.1575	4.5	187.5	30	36.23
122.5	50	0.305	7	125	70	58.14
122.5	350	0.305	7	125	40	45.81
122.5	200	0.305	7	125	47	45.51
63.75	125	0.4525	9.5	187.5	21	25.06
63.75	275	0.4525	4.5	187.5	45	45.65
63.75	275	0.4525	9.5	62.5	9	7.21
122.5	200	0.305	12	125	18	16.97
122.5	200	0.305	7	125	45	45.51
181.25	275	0.4525	4.5	62.5	40	37.80
63.75	125	0.1575	9.5	62.5	10	13.80
122.5	200	0.305	7	0	8.4	8.24
240	200	0.305	7	125	45	44.81
122.5	200	0.305	2	125	49	43.97
181.25	125	0.1575	9.5	187.5	20	23.81
181.25	275	0.1575	9.5	62.5	10	7.96
181.25	275	0.4525	9.5	187.5	45	43.23
181.25	125	0.1575	4.5	62.5	20	23.38
122.5	200	0.01	7	125	14	8.64
5	200	0.305	7	125	25	19.14
63.75	275	0.1575	4.5	62.5	10	10.38
122.5	200	0.305	7	125	55	45.51
181.25	275	0.1575	4.5	187.5	42	42.40
122.5	200	0.305	7	125	40	45.51
181.25	125	0.4525	9.5	62.5	43	44.21
63.75	125	0.4525	4.5	62.5	26	29.63
122.5	200	0.305	7	125	40	45.51
122.5	200	0.305	7	125	40	45.51

controllable parameters. Figure 5 demonstrates that only two factors – pH and the initial dye concentrations – have a significant impact on the dye's ability to bind to surfaces. Additionally, it should be noted that the removal efficiency peaked at low pH and starting dye concentrations.

Transport contaminant and breakthrough curves

The bed in the packaged column contains 1/1 of a mixture of organo-kaolinite and glass waste, so the role of the sand in the remediation process must be established. A contaminant distribution through the packaged bed can be defined by an advection dispersion equation (Figure 6) under the 50 mg/l metal concentration, 50 cm bed depth and 5 mL/min influential water flow rate. By regularizing the concentration of contaminants from the findings already achieved from the experimental values, breakthrough curves were obtained. The point of departure can be described as the time needed for each column test to achieve the highest target contaminant (Cintruent) concentration value at each port. These fronts (or breakthrough dots) will be chosen when the concentration in Figure 6 reaches or exceeds or any desired breakthrough point influential concentrations (50

Table 5. Analysis of variance (ANOVA) for the regression model

Source	DF	Adj SS	Adj MS	F-Value	P-Value
Model	20	7785.02	389.25	6.87	0.001
Linear	5	4885.33	977.07	17.25	0.000
Time (min)	1	988.17	988.17	17.45	0.002
Initial concentration (mg/L)	1	228.17	228.17	4.03	0.070
Dose (g/100mL)	1	1410.67	1410.67	24.90	0.000
pH	1	1093.50	1093.50	19.31	0.001
Agitation speed (rpm)	1	1164.83	1164.83	20.56	0.001
Square	5	2358.19	471.64	8.33	0.002
Time (min)*Time (min)	1	335.93	335.93	5.93	0.033
Initial concentration (mg/L)*Initial concentration (mg/L)	1	76.59	76.59	1.35	0.269
Dose (g/100mL)*Dose (g/100mL)	1	850.33	850.33	15.01	0.003
pH*pH	1	414.50	414.50	7.32	0.020
Agitation speed (rpm)*Agitation speed (rpm)	1	998.41	998.41	17.63	0.001
2-Way interaction	10	541.50	54.15	0.96	0.524
Time (min)*Initial concentration (mg/L)	1	9.00	9.00	0.16	0.698
Time (min)*Dose (g/100mL)	1	156.25	156.25	2.76	0.125
Time (min)*pH	1	30.25	30.25	0.53	0.480
Time (min)*Agitation speed (rpm)	1	0.25	0.25	0.00	0.948
Initial concentration (mg/L)*Dose (g/100mL)	1	0.25	0.25	0.00	0.948
Initial concentration (mg/L)*pH	1	42.25	42.25	0.75	0.406
Initial concentration (mg/L)*Agitation speed (rpm)	1	132.25	132.25	2.33	0.155
Dose (g/100mL)*pH	1	1.00	1.00	0.02	0.897
Dose (g/100mL)*Agitation speed (rpm)	1	1.00	1.00	0.02	0.897
pH*Agitation speed (rpm)	1	169.00	169.00	2.98	0.112
Error	11	623.06	56.64		
Lack-of-fit	6	445.56	74.26	2.09	0.218
Pure error	5	177.50	35.50		
Total	31	8408.08			

mg/L). However, since there is a particular diffusion these points cannot be estimated accurately from experimental evidence and so it is crucial to determining the appropriate representative model for the current test findings. The results of the experiments were modelled (Figures 6). There are the Yan model, the Bohart-Adams model, and the Clark model. They are used to illustrate the breakthrough contaminant curves in the statistical regression column test (Tsvetanova et al., 2022). The parameters of these models corresponding to the research conditions implemented in the present analysis are presented in Table 6. The curves, drawn by these models, are incredibly necessary to know how and how the rate of the front of the contaminant migrates via laboratory column research. The pattern of time treatment in the previously mentioned port, which can later be utilized in the determination of the thickness of permeable reactive barriers, is also identified. The mathematical methods have been utilized with Microsoft Excel 2010 to assess the degree of consensus between the values estimated and evaluated. These mathematical instruments included the decision coefficient (R2). Table 6 lists the R2 values for anticipated and experimental results for the current column samples at various ports. The Clark Model is undoubtedly more representative than other models.

CONCLUSIONS

A new compound called (CTAB-kaolinite) was synthesised and characterised to be used for methyl orange dye removal from industrial wastes by adsorption technique. The research findings showed that total removal percentage

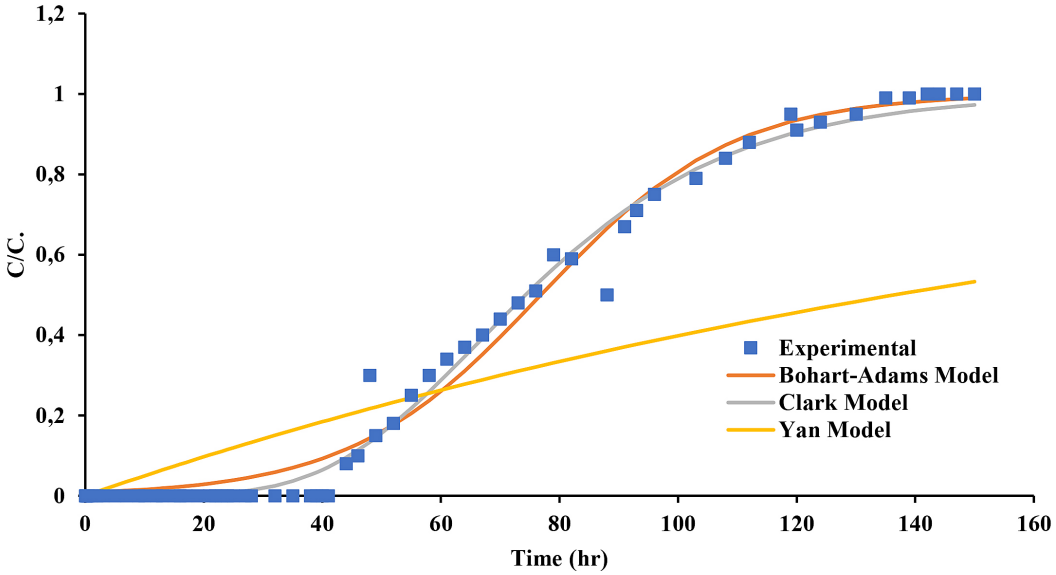

Figure 6. Comparison of the experimental results and breakthrough curves predicted by Clark kinetic model, Bohart-Adams model, and Yan model for migration of methyl orange through bed

Table 6. Constants and statistical measures for breakthrough models

Model	Parameter	Values
Bohart-Adams Model	KC_0	0.061
	$KN_0\frac{Z}{U}$	4.75
	R^2	0.985
	SSE	0.142
Clark Model	*A*	1.590364
	r	$4.29*10^{-2}$
	n	1.091
	R^2	0.989
	SSE	0.096
Yan Model	$\frac{0.001 \times Q \times C}{q_0.M}$	$6.63*10^{-5}$
	a	76.86
	R^2	0.908
	SSE	0.607

was happended at conditions of (contact time: 172 minutes, pH: 4, adsorbent dosage: 0.4 g, dye concentration:50 mg·L^{-1}, and agitation speed: 160 rpm) in which the treatment reactions follows Freundlich and Sips isotherm model efficiently at the equilibrium time in addition to the best kinetics representation by the Pseudo-second-order model. Also, the reliability of the experiment was robust based on the performed ANOVA analysis, revealing the importance of the interplay between the initial dye concentration and pH. This interaction can impact the controll parameters of the removal mechanisms. Moreover, Clark kinetic model yielded satisfactorily agreement for the uptake of the simulated methyl orange during the removal process. Thus, a good effectiveness of using CTAB-kaolinite as an adsorbent in the removal of dyes from water solution was achieved.

REFERENCES

1. Liu Y., Zhu, L. 2017. Enhanced treatment of dispersed dye-production wastewater by self-assembled organobentonite in a one-step process with poly-aluminium chloride. Scientific Reports, 7.

2. Czaja T., Wójcik K., Grzeszczuk M., Szosta, R. 2019. Polypyrrole–Methyl Orange Raman pH Sensor. Polymers, 11, 715. https://doi.org/10.3390/polym1104071
3. Guo X., Wu Z., Wang Z., Lin F., Li P., Liu J. 2023. Preparation of Chitosan-Modified Bentonite and Its Adsorption Performance on Tetracycline. ACS Omega, 8(22),19455–19463. doi: 10.1021/acsomega.3c00745
4. Faisal A.A.H., Al-Wakel S.F.A., Assi H.A., Naji L.A., Naushad M. 2020. Waterworks sludge-filter sand permeable reactive barrier for removal of toxic lead ions from contaminated groundwater. J. Water Process Eng, 33, 101112.
5. Sejie P., Nadiye-Tabbiruka S. 2016. Removal of Methyl Orange (MO) from Water by adsorption onto Modified Local Clay (Kaolinite). Phys. Chem.
6. Demeusy B., Arias-Quintero C.A., Butin G., Lainé J., Tripathy S.K., Marin J., Dehaine Q., Filippov L.O. 2023. Characterization and Liberation Study of the Beauvoir Granite for Lithium Mica Recovery. Minerals, 13, 950. doi: 10.3390/min13070950
7. Ahmed S.N., Ali S.J., Al-Zubaidi H.A.M., Ali A.H., Mohammed A. 2020 . Improvement of organic matter removal in water produced of oilfields using low cost Moringa peels as a new green environmental adsorbent. Global Nest, 22, 268–274.
8. Faisal A.A.H., Naji L.A.2019. Simulation of Ammonia Nitrogen Removal from Simulated Wastewater by Sorption onto Waste Foundry Sand Using Artificial Neural Network. Assoc. Arab Univ. J. Eng. Sci, 26, 28–34.
9. Jeeva M., Zuhairi W.Y.W. 2018. Adsorption of acid orange 33 dye by bentonite and surfactant modified bentonite. Asian J. Chem.
10. Naji L.A., Jassam S.H., Yaseen M.J., Faisal, A.A.H., Al-Ansari, N. 2020. Modification of Langmuir model for simulating initial pH and temperature effects on sorption process. Sep. Sci. Technol, 55, 2729–2736.
11. Abd Ali Z.T., Naji L.A., Almuktar S.A.A.A.N., Faisal, A.A.H., Abed, S.N., Scholz, M., Naushad, M., Ahamad, T. 2020. Predominant mechanisms for the removal of nickel metal ion from aqueous solution using cement kiln dust. J. Water Process Eng, 33, 101033.
12. Alshammari M., Al Juboury M.F., Naji L.A., Faisal, A.A.H., Zhu, H., Al-Ansari, N., Naushad, M. 2020. Synthesis of a Novel Composite Sorbent Coated with Siderite Nanoparticles and its Application for Remediation of Water Contaminated with Congo Red Dye. Int. J. Environ. Res, 14.
13. Al-Zubaidi H.A. 2012. Effect of heavy metals in wastewater effluents of textile factory-Hilla on the characteristics of Hilla River. J. Kerbala Univ, 10, 5–16.
14. Naji L.A., Faisal A.A.H., Rashid H.M., Naushad M., Ahama, T. 2020. Environmental remediation of synthetic leachate produced from sanitary landfills using low-cost composite sorbent. Environ. Technol. Innov, 175, 100680.
15. Anirudhan T.S., Ramachandran M. 2015. Adsorptive removal of basic dyes from aqueous solutions by surfactant modified bentonite clay (organoclay): Kinetic and competitive adsorption isotherm. Process Saf. Environ. Prot, 95, 215–225.
16. Faisal A.A.H., Nassir Z.S., Naji L.A., Naushad M., Ahamad T. 2020. A sustainable approach to utilize olive pips for the sorption of lead ions: Numerical modeling with aid of artificial neural network. Sustain. Chem. Pharm.
17. Kıranşan M., Soltani R.D.C., Hassani A., Karaca S., Khataee A. 2014. Preparation of cetyltrimethylammonium bromide modified montmorillonite nanomaterial for adsorption of a textile dye. J. Taiwan Inst. Chem. Eng, 45, 2565–2577.
18. Fosso-Kankeu E., Waanders F., Fourie C.L. 2016. Adsorption of Congo Red by surfactant-impregnated bentonite clay. Desalin. Water Treat, 57, 27663–27671.
19. Al-Zubaidi H.A.M., Wells S.A. 2020. Analytical and field verification of a 3D hydrodynamic and water quality numerical scheme based on the 2D formulation in CE-QUAL-W2. Journal of Hydraulic Research, 58(1), 152–171. doi: 10.1080/00221686.2018.1499051
20. Faisal A.A.H., Ali I.M., Naji L.A., Madhloom, H.M., Al-Ansari, N. 2020. Using different materials as permeable reactive barrier for remediation of groundwater contaminated with landfill's leachate. Desalin. WATER Treat, 175, 152–163.
21. Ahmed D.N., Faisal A.A.H., Jassam S.H., Naji L.A., Naushad, M. 2020. Kinetic Model for pH Variation Resulted from Interaction of Aqueous Solution Contaminated with Nickel Ions and Cement Kiln Dust. J. Chem, 2020, 1–11.
22. Faisal A.A.H., Jasim H.K., Naji L.A., Naushad M., Ahamad T. 2020. Cement kiln dust-sand permeable reactive barrier for remediation of groundwater contaminated with dissolved benzene. Sep. Sci. Technol, 1–14.
23. Al Juboury M.F., Alshammari M.H., Al-Juhaisi M.R., Naji L.A., Faisal A.A.H., Naushad M., Lima E.C. 2020. Synthesis of composite sorbent for the treatment of aqueous solutions contaminated with methylene blue dye. Water Sci. Technol.
24. Miz M. El, Akichouh H., Salhi S., Bachiri A. El, Tahani A. 2014. Adsorption-desorption and kinetics studies of Methylene Blue Dye on Na-bentonite from Aqueous Solution. IOSR J. Appl. Chem, 7, 60–78.
25. Saad N., Abd Ali Z.T., Naji L.A., Faisal A.A.A.H., Al-Ansari N. 2019. Development of Bi-Langmuir model on the sorption of cadmium onto waste foundry sand: Effects of initial pH and temperature.

Environ. Eng. Res, 25, 677–684.

26. Ahmed M.J., Dhedan S.K. 2012. Equilibrium isotherms and kinetics modeling of methylene blue adsorption on agricultural wastes-based activated carbons. Fluid Phase Equilib, 317, 9–14.
27. Alquzweeni S.S., Al-Zubaidi H.A.M., Samaka I.S., Albahadily, A.R. 2021. Development of a grau model for simulating cephalexin residue removal from wastewater by using lemna minor. Cogent Engineering, 8(1), 1963180. doi: 10.1080/23311916.2021.1963180
28. Naji L.A., Faisal A.A.H., Rashid H.M., Naushad M., Ahamad T. 2020. Environmental remediation of synthetic leachate produced from sanitary landfills using low-cost composite sorbent. Environ. Technol. Innov, 18, 100680.
29. Yan G., Viraraghavan T., Chen, M .2001. A new model for heavy metal removal in a biosorption column. Adsorpt. Sci. Technol, 19, 25–43.
30. Chatterjee A., Schiewer, S. 2014. Multi-resistance kinetic models for biosorption of Cd by raw and immobilized citrus peels in batch and packed-bed columns. Chem. Eng. J. 244, 105–116.
31. Tsvetanova L., Barbov B., Rusew R., Delcheva Z., Shivachev B. 2022. Equilibrium Isotherms and Kinetic Effects during the Adsorption of Pb(II) on Titanosilicates Compared with Natural Zeolite Clinoptilolite. Water, 14, 2152. doi: 10.3390/w14142152
32. Al-Zubaidi H.A.M., Naje A.S., Al-Ridah Z.A., Chabuck A., Ali, I.M. 2021. A Statistical Technique for Modelling Dissolved Oxygen in Salt Lakes. Cogent Engineering, 8(1), 1875533. doi: 10.1080/23311916.2021.1875533
33. Al-Jassani F.D., Al-Zubaidi H.A.M., Al-Mansori N.J. 2022. Satellite-Based Statistical Analysis of Hilla River Water Quality Parameters, Iraq. Nature Environment and Pollution Technology, 21(5), 2315–2321. doi: 10.46488/NEPT.2022.v21i05.027